Phenotypic annotation of the mouse X chromosome

Brian J. Cox,[1,12] Marion Vollmer,[2,12] Owen Tamplin,[1,3,12] Mei Lu,[1] Steffen Biechele,[1,3] Marina Gertsenstein,[4,5] Claude van Campenhout,[2] Thomas Floss,[6] Ralf Kühn,[6] Wolfgang Wurst,[6,7,8,9,10] Heiko Lickert,[2,13] and Janet Rossant[1,3,11,13]

[1]*Program in Developmental and Stem Cell Biology, The Hospital for Sick Children Research Institute, Toronto, Ontario M5G 1L7, Canada;* [2]*Institute of Stem Cell Research, Helmholtz Zentrum München, German Research Center for Environmental Health (GmbH), Neuherberg 85764, Germany;* [3]*Department of Molecular Genetics, University of Toronto, Toronto, Ontario M5S 1A8, Canada;* [4]*Samuel Lunenfeld Research Institute, Mount Sinai Hospital, Toronto, Ontario M5G 1X5, Canada;* [5]*Toronto Centre for Phenogenomics, Transgenic Core, Toronto M5T 3H7, Canada;* [6]*Institute of Developmental Genetics, Helmholtz Zentrum München, German Research Center for Environmental Health (GmbH), Neuherberg 85764, Germany;* [7]*MPI für Psychiatrie, München 80804, Germany;* [8]*Helmholtz Zentrum München, German Research Center for Environmental Health Institute of Developmental Genetics, Neuherberg 85764, Germany;* [9]*Technical University Weihenstephan, Lehrstuhl für Entwicklungsgenetik, c/o Helmholtz Zentrum München, Neuherberg 85764, Germany;* [10]*Deutsches Zentrum für Neurodegenerative Erkrankungen e. V. (DZNE), Standort München, München 80336, Germany;* [11]*Department of Obstetrics and Gynecology, University of Toronto, Toronto, Ontario M5T 3H7, Canada*

Mutational screens are an effective means used in the functional annotation of a genome. We present a method for a mutational screen of the mouse X chromosome using gene trap technologies. This method has the potential to screen all of the genes on the X chromosome without establishing mutant animals, as all gene-trapped embryonic stem (ES) cell lines are hemizygous null for mutations on the X chromosome. Based on this method, embryonic morphological phenotypes and expression patterns for 58 genes were assessed, ~10% of all human and mouse syntenic genes on the X chromosome. Of these, 17 are novel embryonic lethal mutations and nine are mutant mouse models of genes associated with genetic disease in humans, including *BCOR* and *PORCN*. The rate of lethal mutations is similar to previous mutagenic screens of the autosomes. Interestingly, some genes associated with X-linked mental retardation (XLMR) in humans show lethal phenotypes in mice, suggesting that null mutations cannot be responsible for all cases of XLMR. The entire data set is available via the publicly accessible website (http://xlinkedgenes.ibme.utoronto.ca/).

[Supplemental material is available online at http://www.genome.org. Phenotype data and images of analyzed cell lines have been submitted to Mouse Genome Informatics (http://www.informatics.jax.org) under the allele IDs listed in Supplemental Table 2.]

X-linked genetic disorders play a major role in the impact of Mendelian traits on human health. The human X chromosome contains only 4% of all annotated genes (1098) (Ross et al. 2005), but nearly 10% of all known Mendelian diseases in the Online Mendelian Inheritance in Man (OMIM) database are linked to the X chromosome (387/3983), as of October 2009. It has been suggested that this may be due to a discovery bias (Ross et al. 2005). Most of these traits disproportionately affect males, where there is only one copy of the mutant X chromosome. Females can often escape severe effects of these mutations because X inactivation renders them functionally mosaic. Alternatively, the X chromosome carrying the mutated allele is preferentially inactivated (Garrick et al. 2006). Of these X-linked diseases, 30% (149/387) are not mapped to a mutation in a specific gene. In addition, embryonic lethal mutations in X-linked genes are thought to underlie the preferential loss of male embryos in many cases of recurrent spontaneous abortion (RSA) (Pegoraro et al. 1997; Lanasa et al. 2001). Clearly, there is a need to better understand the function of genes on the X chromosome in order to link them to the full range of human X-linked disorders.

[12]These authors contributed equally to this work.
[13]Corresponding authors.
E-mail janet.rossant@sickkids.ca.
E-mail heiko.lickert@helmholtz-muenchen.de.
Article published online before print. Article and publication date are at http://www.genome.org/cgi/doi/10.1101/gr.105106.110.

Comparative analysis of the mouse and human genomes reveals that there is a high degree of conservation and synteny between the X chromosomes, with 90% of known genes (629/699) conserved (Ross et al. 2005). The ability to genetically manipulate the genome in mouse embryonic stem cells (mESC) makes it possible to generate mouse models of human X-linked disorders. However, phenotypic analysis of such mutations to date has been slow, because of the frequent difficulties in generating high-percentage chimeras with hemizygous XY mESCs and transmitting the mutant X-linked allele through the germ line. There are 211 targeted mutant phenotypes on the mouse X chromosome reported in the Mouse Genome Database (http://www.informatics.jax.org/phenotypes.shtml), 50 of which are associated with a human disorder. However, the efforts of the International Gene Trap Consortium (IGTC) (Nord et al. 2006) and the International Knockout Mouse Consortium (IKMC) (International Mouse Knockout Consortium 2007) have placed a growing resource of mutant mESC lines in the public domain. As of January 2010, 473 of the genes on the mouse X chromosome are now associated with either a gene trap (379 genes) or targeted mutant cell line. As a means of identifying novel disease genes, the mouse gene trap (GT) resource can be mined for insertions in genes with human X-linked orthologs that have yet to be associated with developmental processes in either mice or humans.

Using a straightforward approach of generating and analyzing mESC-derived embryos, we have added embryonic phenotypic

20:1154–1164 © 2010 by Cold Spring Harbor Laboratory Press; ISSN 1088-9051/10; www.genome.org

and functional data to almost 10% of syntenic genes on the mouse X chromosome. This rapid and cost-effective screening method has identified 19 (13 novel to mouse and human) X-linked mutations that cause developmental defects in the mouse and are therefore likely to cause human congenital disease. These embryonic abnormalities occur during gastrulation, neurulation, and organogenesis and include phenotypes such as neural tube closure defects, axis truncation, cardia bifida, and heart failure, all leading to early embryonic lethality. Moreover, the beta-galactosidase (*lacZ*) reporter gene introduced by the GT vector insertion provided gene expression information of value in predicting gene function.

Two of the embryonic lethal phenotypes resulted from mutations in the genes BCL6 interacting corepressor (*Bcor*) and the Wnt-ligand modifier porcupine homolog (*Porcn*). Interestingly, after the start of our screen, these genes were associated with X-linked diseases in humans: oculofaciocardiodental syndrome (OFCD) (OMIM:300166; *BCOR*) (Ng et al. 2004) and focal dermal hypoplasia (FDH) (OMIM:305600; *PORCN*) (Grzeschik et al. 2007; Wang et al. 2007). In both cases symptomatic human females survive into adulthood, but fully hemizygous null males are never observed (Ng et al. 2004; Grzeschik et al. 2007; Wang et al. 2007). We show that GT mutants for *Porcn* fail to complete gastrulation, while *Bcor* GT mutants have severely affected heart development. This provides proof-of-principle of the utility of mutagenic screens in the mouse to identify candidate genes for human disease.

Recent resequencing of the coding exons of the human X chromosome identified few novel candidates for X-linked mental retardation (XLMR), indicating that XLMR may be due to mutations in gene regulatory regions rather than coding regions. We observe that many of the known XLMR genes assessed in our screen have lethal phenotypes when null in the mouse, suggesting that human XLMR may be caused by hypomorphic rather than null mutations. To facilitate disease candidate data mining between human and mouse phenotypes, expression patterns, and genetic loci, we have compiled our data set into an online relational database (http://xlinkedgenes.ibme.utoronto.ca/), along with human data from OMIM.

Results

The genotype-driven screen

The protocol for choosing GT mESC lines is summarized in Figure 1A and detailed in the Methods section. Briefly, sequence tags for trapped genes were aligned against transcripts that localize to the X chromosome. Those that aligned were selected based on deleting >50% of the gene (exceptions were made if no alternate traps were available). Finally, genes were filtered for reports of mutagenesis in the mouse or linkage to a human disease as of September 2004, when the screen began. Two genes that are linked to human diseases, *Atrx* and *Flna*, were included as positive and negative controls. Null mutations in *ATRX* have no embryonic lethality in humans, while null mutations in *FLNA* cause embryonic male lethality. A total of 68 GT cell lines representing 58 genes were aggregated with wild-type embryos to generate mESC-derived embryos for phenotypic analysis (Table 1; Fig. 2). While the focus of the screen was to identify novel human disease candidates, several human disease alleles were mapped during the course of the screen (Fig. 2, human genes in bold).

Two different aggregation techniques were used to generate embryos that were derived completely from the GT mESC lines: aggregation with tetraploid (Nagy et al. 1990) and diploid (Nagy et al. 1990; Poueymirou et al. 2007) eight-cell stage embryos, with the exception that we aggregated rather than injected cells under the zona (see Methods; Fig. 1B). While the two techniques produce comparable numbers of mESC-derived embryos, tetraploid aggregation requires twice as many host embryos as diploid aggregation, since two embryos are aggregated with a clump of mESCs. We noted similar rates of embryo implantation and mESC-derived embryos regardless of genetic background or source of cell line (Supplemental Table 1). At mouse mid-gestation stage (embryonic day [E9.5]; equivalent to human week 5), the fully mESC-derived embryos were fixed and stained for *lacZ* expression (Fig. 1B), then imaged and assessed for phenotype and expression pattern. At this stage, the basic body plan is laid down, patterning of the nervous system is apparent, and organogenesis has begun. It thus provides an effective developmental stage to compare human and mouse development, gene expression patterns, and mouse mutant phenotypes relevant to human congenital disease. All image and text information has been placed in a relational database (Fig. 1B). The entire data set includes results from 128 different aggregation experiments that generated over 1200 fully mESC-derived embryos (Table 1).

Phenotypes and gene expression patterns

Figure 2 summarizes the genes analyzed in our screen and their phenotypes and expression patterns. In total, 26 cell lines representing 19 genes were scored as having a phenotype in the mouse embryo by E9.5 (Fig. 2, mouse genes in bold). Of these 19 phenotypes, 17 are novel mouse phenotypes where no mutants have been reported in the literature. Thirteen of the novel mouse mutants have no reported mutations in human homologs, making them candidate human disease loci. The remaining 38 genes had no obvious morphological phenotype by E9.5. Aggregation of the parental lines E14 and R1 by either tetraploid or eight-cell-stage diploid embryos produced healthy and normal embryos at E9.5 (data not shown).

For assessment of phenotypes we considered the developmental processes completed or in progress by E9.5, then classified the observed phenotypes into several broad categories (Table 2). The majority of phenotypes fell into the classes of turning, neurulation, cardiogenesis, and axial growth (i.e., somitogenesis and posterior axis elongation). Several genes were scored with a gastrulation phenotype (i.e., formation of the basic body plan and three germ layers), and showed arrested development or altered morphology. Only one GT mESC line did not yield any gastrulation-stage embryos, possibly because the mutated gene, cytochrome *c* oxidase subunit VIIb, produces an enzyme for general energy metabolism of cells, although mESC are viable (Table 2; *Cox7b*).

We also scored expression of the *lacZ* GT reporter in the embryos. Of the lines with embryonic phenotypes, 15 had expression of *lacZ* at the stages observed, with six restricted and nine ubiquitous expression patterns (Fig. 2, expression information and database). Three cell lines had no *lacZ* staining: *Cul4b*, *Rbm3* (no *lacZ* reporter), and *Porcn* (insertion before the start codon). Of the GT mutations without a phenotype at E9.5, 13 had restricted expression patterns, four were widespread, nine were ubiquitous, and 10 had no expression (Fig. 2). Lack of a phenotype at E9.5 does not preclude later effects, which were beyond the scope of this study, but the observation of expression restricted to particular tissues at E9.5 can be used to focus future phenotypic analysis of mutant mouse lines.

To assess the robustness of the screening method, we aggregated at least two independent lines for 11 genes (Fig. 2, replicates).

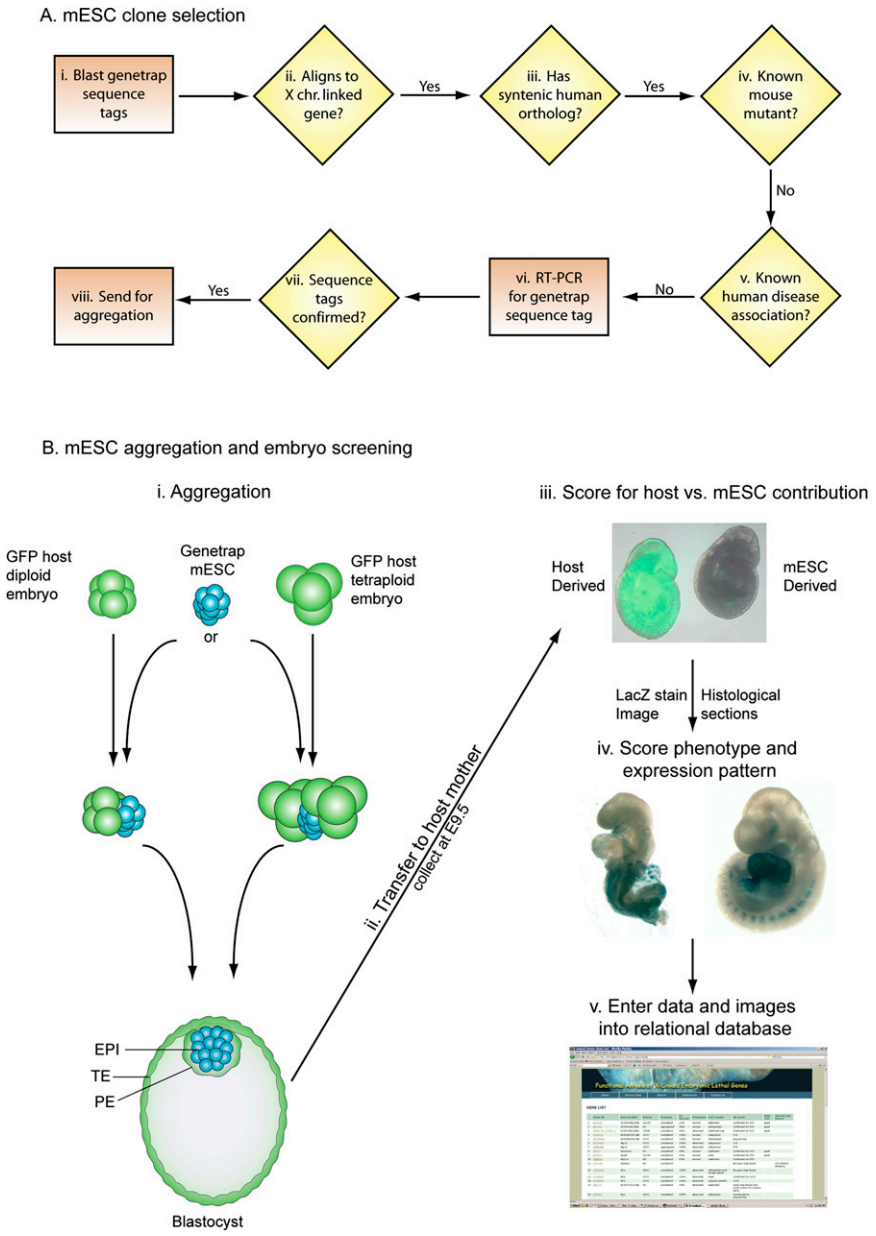

Figure 1. An overview of the screening method. (*A*) mESC GT clone selection involved blasting of sequence tags to transcripts from the X chromosome (*i*). All BLAST (Altschul et al. 1990) hits >95% identical were then compared with the human X chromosome (*ii*). Those genes with a syntenic homolog were then filtered for any known mouse mutants and known links to human disease (*iv*,*v*). GT lines were ordered and quality controlled by RT-PCR to confirm the sequence tag prior to aggregation (*vii*,*viii*). (*B*) Two different aggregation techniques (*i*) were used with similar results and efficiency (Table 1). mESCs were aggregated with either one diploid or two tetraploid host embryos and cultured overnight. After overnight culture, the colony of mESC preferentially forms the epiblast of the embryo and displaces the host cells to the primitive endoderm and trophectoderm of the blastocyst. mESCs contribute only to the epiblast (EPI) that will generate the embryo proper, while the host (all tetraploid and a large proportion of diploid) embryos generate the primitive endoderm (PE) and the trophectoderm (TE). Aggregated embryos were transferred to pseudopregnant mothers and collected at E9.5 (*ii*). Dissected embryos were scored for mESC contribution by observing GFP fluorescence (*iii*). The embryo on the *left* is GFP positive and has diploid host embryo contribution, while the embryo on the *right* is GFP negative and is fully mESC-derived (*iii*). Fully mESC-derived embryos were fixed and stained for beta-galactosidase (*lacZ*) activity. After staining, the embryos were digitally imaged and scored for expression and phenotype (*iv*). All digital images and aggregation data were entered into a relational database (*v*).

In 10 out of 11 cases the resulting replicates had highly similar phenotypes (Fig. 2). Several of the GT lines used in this screen contained conditional multipurpose alleles that can be inverted using site-specific recombination to restore wild-type function (Schnutgen et al. 2005). The loss-of-function *Nono* GT mESC line presented a strong gastrulation phenotype, with developmental arrest at E7.5. We confirmed specificity of the phenotype by Cre-mediated GT inversion, rescue of gene function, and restoration of Nono protein to normal levels (Supplemental Fig. 1). Furthermore, embryos derived from inversion-rescued GT lines were phenotypically normal at E9.0 (n = 10; Supplemental Fig. 1). Although we did not test all GT lines similarly, the results of the redundant lines, the high correlation of phenotype and *lacZ* reporter expression, and the inversion of the GT demonstrate that the screen was robust. There is high confidence that the observed phenotypes are the results of the GT mutations and not nonspecific effects associated with particular mESC clones.

Relationship of embryonic phenotypes to human disease genes

Although our screen was intended to focus on genes with no known phenotype in mouse or human, several human homologs were linked to human diseases during the course of our screen. Two of the GT lines assayed in our screen recapitulated known human diseases with embryonic lethality in male embryos: *Bcor* and *Porcn*. BCOR is a transcriptional repressor that has been described to affect levels of histone H3 K4 trimethylation (activated gene mark) (Fan et al. 2009) and physically interact with histone demethylases (Sanchez et al. 2007). The human homolog of mouse *Bcor* is associated with OFCD (OMIM:300166) (Ng et al. 2004). We generated fully mESC-derived mutant embryos from three different GT lines of *Bcor*: one in intron 1c (P101H07) and two in intron 5 (DB0053 and XE541, the latter was used in the study by Wamstad et al. 2008) (Fig. 3A). Based on cap-analysis gene expression (CAGE) tag analysis of the *Bcor* locus, there are two alternate transcriptional start sites in the first exon and two more in the fourth exon (Fig. 3A; Kawaji et al. 2006). Thus, a GT in the first intron would not trap all alternative transcripts, but the two GTs inserted after exon 5 would, possibly causing a more severe phenotype (Fig. 3A). To test this idea, we analyzed and compared all three *Bcor* GT lines.

Table 1. Total numbers of embryos processed during screen of 68 gene trap cell lines for 58 genes

Method	Tested cell lines	Experiments	Transferred embryos	Recovered embryos	Fully ES-derived embryos
Delayed diploid	41	54	4663	1647	645
Tetraploid	27	74	2850	768	630
Total	68	128	7513	2415	1229

Bcor GT lines DB0053 and XE541 both show lethality by E9.5 with apparent fusion of the ventral forebrain, greatly reduced and malformed cardiac tissue, and severe posterior truncation with failure of chorioallantoic fusion (cf. Fig. 3B,C,D and Q,R). Consistent with the phenotype, *lacZ* reporter staining was observed strongly in the head, heart, and tail bud at E8.5 (Fig. 3B,C). Embryos derived from both GT lines showed variable numbers of cysts along the dorsal region flanking the neural tube and occasionally in the head region (Fig. 3C; data not shown). Histological sections through the head revealed the eyes to be either delayed in formation or missing completely (cf. Fig. 3F and G, star). Histological sections through the heart showed a bilateral symmetrical heart, compared with the looped asymmetrical heart of similarly staged wild-type controls (cf. Fig. 3H and I). At this level of analysis it is not clear if this is a result of failed looping or cardia bifida. These results clearly indicate that different GT mESC lines give reliable and consistent embryonic phenotypes.

GT line P101H07 displayed a less severe phenotype with an open head and delayed cardiac folding, but a more elongated tail region, proper chorioallantoic fusion, and normal optic cup anlage (Fig. 3E; data not shown). These results demonstrate that a GT line is a valuable resource to mutagenize splice-specific and promoter-specific isoforms, and that this can generate tissue-specific phenotypes with different levels of severity.

We aggregated a GT cell line for *Porcn* for which the human homolog is associated with FDH (OMIM:305600) (Grzeschik et al. 2007; Wang et al. 2007). The *PORCN* gene encodes a membrane-bound O-acyl transferase (MBOAT) that is involved in the acyl modification of Wnt ligands, which is important for long-range signaling (Tanaka et al. 2000). The GT insertion for *Porcn* lies between the first and second exons before the translational start codon (Fig. 3J), truncating the entire coding region of the transcript (as confirmed by RT-PCR; data not shown). *Porcn* null embryos were observed from E7.5 to E9.5 (Fig. 3K–M), but embryonic development arrested during gastrulation, with no recognizable anterior–posterior axis based on morphological landmarks, such as head fold or allantois (cf. Fig. 3K and P). Histological sections at E7.75 (Fig. 3O,T) revealed that the mutant epiblast accumulated in the amniotic cavity, and there was a marked absence of the allantois (data not shown).

Epiblast overgrowth may be a result of a failure of the epiblast to differentiate. To assess the differentiation state of the *Porcn* mutant epiblast, we assayed the RNA expression of *Pou5f1* (*Oct3/4*) as a marker of pluripotency by whole mount in situ hybridization. Compared with E8.0 controls, where *Pou5f1* was sufficiently down-regulated and epiblast cells started to differentiate (Fig. 3S), *Porcn* GT mutants showed prolonged expression indicating a lack of differentiation (Fig. 3N). This is very similar to *Wnt3* (Liu et al. 1999) and beta-catenin (Morkel et al. 2003) mutants, which fail to undergo EMT and lack mesoderm and endoderm. The *Porcn* GT mutant embryos are phenotypically similar to *Wnt3* mutants (the earliest Wnt phenotype), which supports accumulating evidence that *Porcn* is required for the secretion of WNT. More detailed analysis of anterior–posterior axis patterning genes is needed to confirm this phenotype. Our observations provide insight into the cause of male embryonic lethality in humans with *PORCN* mutations.

There were seven additional known human X-linked disease genes where human mutations are viable, but for which we report an embryonic phenotype; four of these are described here for the first time (*Brwd3*, *Cul4b*, *Huwe1*, and *Kdm5c* (formerly *Jarid1c*); Table 3), while the others have been previously published (*Atrx*, *Dlg3*, *Flna*; Table 3). In many cases the GT line was a null allele, while no null alleles have been found in the human pathologies (Table 3). For example, mutations in *CUL4B* are associated with Cabezas syndrome (OMIM:300354) and mental retardation (MRX 15, OMIM:300639). We analyzed a GT resulting in a null mutation for *Cul4b* and observed incomplete turning, defective neurulation, shortened posterior axis, swollen pericardium, and stalled cardiac development. In humans with Cabezas syndrome (*CUL4B*), all reported mutations are C-terminal truncations. As the null mutation has not been observed in humans, this strongly suggests that a null allele may also cause early gestational lethality in humans.

Novel early embryonic lethal genes

We observed 17 novel embryonic mutant phenotypes in X-linked genes that exhibited a wide range of defects and had no previous mutation reported in mice (Table 2). As noted above, 13 of these have no reported mutations in human homologs and therefore represent novel candidates for human disease loci. We present a focused morphological assessment of three candidates, one from each phenotype class of cardiac development, neurulation, and axis formation.

Of the genes giving cardiac defects, the mutation in *Alg13* was the most striking, causing cardia bifida where the two heart primordia remain separate and form two hearts on either side of midline (Fig. 4A,B). This cardiac defect is typically due to defects in foregut development resulting in failure of the cardiac precursors to meet at the midline. ALG13 is a soluble cytosolic protein recruited to the endoplasmic reticulum (ER) to form a heterodimer with the ER membrane protein ALG14 (Gao et al. 2005). Together, they generate a UDP-GlcNAc glycosyltransferase that catalyzes the second sugar addition in the synthesis of the dolichol-linked oligosaccharide precursor in N-linked glycosylation (Gao et al. 2005). The exact enzymatic targets of the ALG13/14 complex are unknown, but several protein ligands (i.e., WNTs, SHH) and transmembrane receptors require N-linked glycosylation for proper function.

In *Kdm6a* (formerly *Utx*) mutant embryos we observed restricted GT *lacZ* reporter gene expression in the neuroectoderm of the brain and neural tube at E9.5 (Fig. 4C). The embryos showed exencephaly in the mid- and hindbrain region. Histological sections through the head showed that the forebrain vesicle fails to fuse in the rostral region and the optic pits are asymmetrical as compared to control embryos (cf. Fig. 4D and J, stars). KDM6A has been identified as a histone H3 K27 demethylase involved in epigenetic regulation of gene expression (Lee et al. 2007). *Kdm6a* also escapes X inactivation in both the mouse and human (Greenfield et al. 1998).

Expression of *Ccdc160* in mutant embryos was first observed in the node at E7.5 (Fig. 4E; Supplemental Fig. 2A,E) and in the neural tube at E9.5 (Fig. 4F). At E9.5, *Ccdc160* mutant embryos had

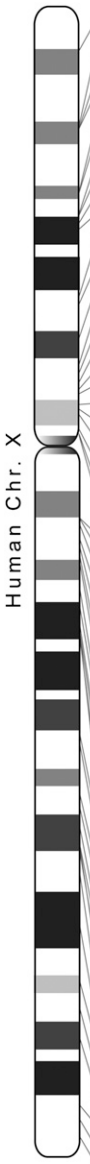

Cytoband	Human Gene	Mouse Gene (replicates)	Expression
Xp22.32	*SFRS17A*	***Sfrs17b***	Brain, neural tube
Xp22.2	*PIR*	*Pir*	Brain, gut tube
Xp22.2	*SYAP1*	*Syap1*	Widespread
Xp22.2	*CXorf15*	*4932441K18Rik*	Ubiquitous
Xp22.2	*RAB9A*	*Rab9*	NE
Xp22.2	*RBBP7*	***Rbbp7***	Ubiquitous
Xp22.12	*CXorf23*	*A830080D01Rik* (2/2)	Ubiquitous
Xp22.12	*MAP7D2*	*Mtap7d2*	Brain, eyes, neural tube
Xp22.1	*POLA1*	*Pola1*	Widespread
Xp22	*CTPS2*	*Ctps2*	Hepatic bud, gut tube
Xp21.2	*TAB3*	*Tab3*	Heart, somites, brain, eyes
Xp21.2	***BCOR***	***Bcor*** (3/3)	Brain, heart, tail bud
Xp11.4	*MED14*	*Med14*	Ubiquitous
Xp11.4	*USP9X*	***Usp9x*** (1/2)	Ubiquitous
Xp11.3	*PHF16*	*Phf16*	Rhombomeres, gut tube
Xp11.23	*FTSJ1*	*Ftsj1*	NE
Xp11.23	***PORCN***	***Porcn***	NE
Xp11.23	*GLOD5*	*Glod5*	Yolk sac mesoderm
Xp11.23	*OTUD5*	***Otud5***	Ubiquitous
Xp11.23	*WNK3*	*Wnk3*	NE
Xp11.23	*RBM10*	*Rbm10*	Ubiquitous
Xp11.22	***KDM5C***	***Kdm5c*** (2/2)	Widespread
Xp11.22	***HUWE1***	***Huwe1*** (3/3)	Ubiquitous
Xp11.22	*FAM120C*	*Fam120c*	NE
Xp11.21	*KLF8*	*Klf8*	Heart
Xp11.2	*KDM6A*	***Kdm6a***	Lung bud, limb, neural tube
Xp11.2	*RBM3*	***Rbm3*** (2/2)	No LacZ
Xq13	*OGT*	*Ogt*	NE
Xq13	*CHIC1*	*Chic1*	NE
Xq13	*RLIM*	*Rlim*	Ubiquitous
Xq13.1	***DLG3***	***Dlg3***	Ubiquitous
Xq13.1	*KIF4A*	*Kif4*	Neural tube, brain, heart
Xq13.1	*SNX12*	*Snx12*	Widespread
Xq13.1	*NONO*	***Nono*** (2/3) #	Ubiquitous
Xq13.1	*TAF9B*	*Taf9b*	NE
Xq13.1	***ATRX***	*Atrx* (2/2)	Widespread
Xq13.3	*ZDHHC15*	***Zdhhc15***	Neural tube
Xq21	*RPS6KA6*	***Rps6ka6***	Lateral plate mesoderm, ear
Xq21.1	*COX7B*	***Cox7b***	NA
Xq21.1	***BRWD3***	*Brwd3*	Brain, heart, gut tube
Xq21.1	*HDX*	*Hdx*	Ubiquitous
Xq21.1	*APOOL*	*Apool*	NE
Xq22	*DIAPH2*	*Diap2* (2/2)	Heart, somites
Xq22.1	*RBM41*	***Rbm41***	Widespread
Xq22.1	*RAB9B*	*Rab9*	NE
Xq22.3	*AMMECR1*	*Ammecr1*	Thymus, thyroid, parathyroid
Xq23	*ALG13*	***Alg13*** (2/2)	Ubiquitous
Xq23	*LRCH2*	*Lrch2*	Brain, neural tube, eyes
Xq23	*CXorf56*	*C330007P06Rik* (2/2)	Brain, eyes, neural tube
Xq23	***CUL4B***	***Cul4b***	NE
Xq24	*WDR44*	*Wdr44*	Somites
Xq25	*ENOX2*	*Enox2*	Heart
Xq26.2	*CCDC160*	***Ccdc160***	Node, neural tube
Xq26.3	*FAM122B*	*Fam122b*	Heart
Xq27.1	*ATP11C*	*Atp11c*	Brain, gut tube
Xq28	*PDZD4*	*Pdzd4*	NE
Xq28	*VBP1*	*Vbp1*	Ubiquitous
Xq28	***FLNA***	*Flna*	Ubiquitous

Figure 2. Linkage to human homologs and summary of expression and phenotype. The human orthologs of the mouse GT genes are aligned to their cytoband on an ideogram of the human X chromosome. Also shown are the names of human and mouse homologs and a brief summary of the observed expression pattern of the beta-galactosidase reporter gene in the embryos. (Bold mouse genes) Gene names for GT lines that gave a phenotype. Eleven mouse genes were tested by two or more GT lines and are indicated in parentheses next to the mouse gene name as a ratio of lines with similar expression or phenotype. The phenotype for the gene *Nono* was confirmed by inverting the GT and restoring *Nono* expression and normal phenotype in aggregated embryos (#). (Bold human genes) Names associated with human disease or syndromes when mutated.

a severe truncation of the posterior body axis (cf. Fig. 4F and I). Histological analysis of *lacZ* expression revealed highly restricted expression in the ventral neural tube (Fig. 4G,H). The neural epithelium was disrupted bilaterally in three out of three embryos examined (cf. Fig. 4G,H and K,L; data not shown). The posterior truncation and other defects may result from the expression and function of *Ccdc160* in the node, which gives rise to the notochord and is required for dorsal–ventral patterning of the neural tube as well as trunk and tail organizers (Yamanaka et al. 2007). Moreover, a weak and transient expression of the *lacZ* reporter was observed in the late streak at E7.5 (Supplemental Fig. 2B–D), which suggests a role for *Ccdc160* in posterior mesoderm development. The gene codes for a small protein of 323 amino acids with no known domains aside from a putative coiled-coil domain that is a common feature of centrosome/basal body proteins (Andersen et al. 2003). Interestingly, *Ccdc160* is expressed in regions of high Shh signaling (i.e., node and ventral neural tube), which in mammals depends on primary cilia. Genomic BLAST analysis showed that the gene *Ccdc160* and its homologs are found only in mammals, including opossum and platypus, perhaps indicating that *Ccdc160* is an evolutionary adaptation to mammalian development.

Online database

Data on aggregation efficiency and images of mESC-derived embryos are available on a publicly accessible website (http://xlinkedgenes.ibme.utoronto.ca/). The database is searchable by gene name or can be browsed. We have integrated our image and text data of these mutant embryos with the OMIM database. As mentioned in the introduction, there are over 140 suspected X-linked diseases that have not been mapped to a specific gene. To facilitate data mining we have extracted these OMIM entries and entered them into our database, placing all mouse GTs for orthologous human genes within the defined linkage regions for OMIM entries on the human X chromosome. Constraints can be placed on either the expression pattern or phenotype of the mouse homologues to find those similar to the human disease or syndrome. Phenotype data and images of analyzed cell lines have been deposited with MGI (http://www.informatics.jax.org). MGI allele IDs for each of the characterized lines can be found in Supplemental Table 2.

Discussion

Using publicly available GT insertion mESC lines and a rapid and cost-effective phenotypic assay based on generating entirely mESC-derived embryos, we have added functional annotation to almost 10% of mouse syntenic X-linked genes and provided an online resource to link mouse phenotype and expression information to human disease.

It has been suggested that the observation of a higher percentage of Mendelian genetic diseases being linked to the X chromosome is a discovery bias (Ross et al. 2005) based on the ease of detection of X-linked phenotypes in males and, in some cases, in

Table 2. Genes scored as having a morphological phenotype

Gene symbol	Human mutation	Novel mouse mutant	Phenotype class					
			Implantation	Gastrulation	Turning	Neurulation	Axial/ trunk	Cardiogenesis
Ccdc160		This study		✓		✓	✓	✓
Alg13		This study			✓	✓	✓	✓
Sfrs17b		This study				✓	✓	
Bcor	Yes	Wamstad et al. 2008				✓	✓	✓
Cox7b		This study	✓					
Cul4b	Yes	This study			✓	✓	✓	✓
Dlg3	Yes	Cuthbert et al. 2007			✓	✓	✓	
Huwe1	Yes	This study		✓	✓	✓	✓	
Kdm5c	Yes	This study				✓		✓
Nono		This study		✓				
Otud5		This study			✓	✓	✓	
Porcn	Yes	This study		✓				
Rbbp7		This study			✓			✓
Rbm3		This study			✓		✓	
Rbm41		This study				✓		
Rps6ka6		This study			✓		✓	
Usp9x		This study			✓	✓		✓
Kdm6a		This study				✓	✓	
Zdhhc15		This study				✓		

X-inactivation mosaic females. In our unbiased screen for embryonic phenotypes in X-linked GT mutations in the mouse, we have detected about 32% (19/58) with an early developmental phenotype. This is in line with other GT-based mutagenesis studies that focused on the autosomes, where 33% (Mitchell et al. 2001) and 37% (Friedrich and Soriano 1991) of genes tested presented phenotypes. This assessment does come with the caveat that we have included both recessive and dominant phenotypes of the previous gene trap screens. We justify this by the fact that our screen is a hemizygous null so we cannot discriminate recessive from dominant mutations in our screen. Thus, we conclude from our analysis that autosomal and X-chromosomal-lethal phenotypes occur at similar rates.

Importantly, as a proof-of-principle we confirmed early male embryo lethality in two mouse models, *Bcor* and *Porcn*, where lethality in humans was only suspected. *BCOR* mutations are associated with human OFCD (OMIM 300166) (Ng et al. 2004). Human males do present with OFCD when *BCOR* has a hypomorphic mutation such that some functional protein is made (Hilton et al. 2009). *Bcor* mutants have previously been generated in the mouse and, although no hemizygous null males were observed postnatal, there was no assessment of the embryonic phenotype (Wamstad et al. 2008). We clearly demonstrate that *Bcor* has an essential function during embryonic development and we offer an explanation for male embryonic lethality.

Mutations in *PORCN* are associated with human FDH (OMIM:305600) (Grzeschik et al. 2007; Wang et al. 2007). The majority of patients are female, and only males with mosaic spontaneous somatic mutations are viable, indicating that hemizygous null males die during gestation (Grzeschik et al. 2007; Wang et al. 2007). Patients present with lateral skin lesion and hair loss, fused and extra digits, mental retardation, microphthalmia, and dental and palate disorders (Grzeschik et al. 2007; Wang et al. 2007). Our data demonstrate that *Porcn* mutants phenocopy known *Wnt*/beta-catenin mutants and that *Porcn* is essential for epiblast differentiation, as *Pou5f1* expression was not down-regulated. This embryo morphology is very similar to Wnt3 mutants, the earliest of Wnt mutant phenotypes (Liu et al. 1999), which fail to undergo EMT and lack mesoderm and endoderm. Taken together, our observations support accumulating evidence that *Porcn* is required for the secretion of functional Wnt proteins and provide a cause/mechanism for male embryonic lethality in humans. From the analysis of *Bcor* and *Porcn* we conclude that our screen can identify embryonic phenotypes that can give insight into key developmental pathways associated with postnatal disease.

Although the screen was designed to identify mid-gestation lethal mutations, we also observed many embryos with a normal morphology, even though the trapped genes showed clear expression by *lacZ* reporter at and before E9.5. It is possible that loss of function of these genes could be compensated by the coexpression of close paralogs or that the phenotype may not be overtly apparent at this stage. Of the genes that were observed to have cardiac expression, for example, many were in the trabecular cells, which are only just developing at E9.5. Defects in trabecular formation may not be phenotypically or even morphologically apparent until later in gestation. An example of this was *Klf8*, which had expression in the left side ventricle and outflow tract. Interestingly, the human homolog *KLF8* maps to the locus of the human syndrome TARPS (Kurpinski et al. 2003) that has left side cardiac defects. Unfortunately, sequencing of the coding regions of *KLF8* in two families did not reveal any mutations in the coding regions; however, mutations in the promoter or enhancers have not been tested (L Biesecker, pers. comm.).

Another common class was genes with expression in the developing brain; these could be associated with XLMR, which would not be apparent until postnatal time points. For example, *Brwd3*, which was associated with XLMR by another group during the course of our study (Field et al. 2007), has *lacZ* reporter expression in the brain and neural tube. Expression does not have to be restricted; an example of this from our screen is *Dlg3*, where in humans mutations in *DLG3* are associated with mental retardation (Tarpey et al. 2004). Aggregation results from mESC line with a gene-trap insertion in *Dlg3* (clone P038A02) revealed ubiquitous expression of *lacZ* and showed a range of phenotype severity. Embryo phenotypes for *Dlg3* mutants ranged from morphologically normal to failure of embryonic turning (five out of 18), including rare cases with forebrain deletion (one out of 18). This GT phenotype has been confirmed using a *Dlg3* KO mouse line in an inbred background (C van Campenhout, P Giallonardo,

C Gloeckner, A Eitelhuber, M Gegg, S Grant, D Krappmann, M Ueffing, and H Lickert, in prep.). The mouse phenotype indicates a critical role for *Dlg3* in neural induction and that non-null mutations could cause more subtle developmental defects leading to cognitive deficiencies. The partial penetrance of this phenotype suggests that alleles of other genes could modify the penetrance of the mutant phenotype.

A large-scale resequencing of the X chromosome in families with XLMR found few novel genes with exonic mutations that could be associated with mental retardation (Tarpey et al. 2009). A possible explanation is that the causative mutations are in regulatory elements or splicing control regions; a difficult prospect for sequence analysis. This is indirectly supported by our observation that some human XLMR genes had lethal phenotypes when null in the mouse (*Cul4b*, *Dlg3*, *Huwe1*, *Kdm5c*; Table 3). Thus, it is possible that null mutations give rise to early embryo lethality, but tissue-specific loss of gene expression caused by mutations in regulatory regions may cause XLMR. We suggest that mutagenic screens in the mouse, such as this current study, may be used to identify genes with expression patterns or phenotypes consistent with a function in brain or neural development. These genes would be candidates for more focused resequencing efforts.

The screening method used here does not rely on the generation of founder animals, extensive crossing schemes, or mapping of mutations. Instead, preselection and testing of candidate disease genes can be carried out in a very short time frame. Generation of mESC-derived embryos was first reported by aggregation of mESC with tetraploid embryos (Nagy et al. 1990), a technique also used in part of our screen. However, a subsequent report suggested that laser-assisted injection of mESCs under the zona pellucida of diploid eight-cell embryos could also generate mESC-derived mice at an efficient rate (Poueymirou et al. 2007). In this study, we used an aggregation method with diploid eight-cell embryos and were able to generate completely mESC-derived embryos with similar success to aggregation with tetraploid embryos. Eliminating the need for electrofusion or laser-assisted injection simplified the method and dramatically reduced labor and cost of the assay. The majority of GT lines were generated using a vector that only traps genes expressed in mESCs, thus limiting the genes available for analysis. However, newer GT lines from the Center for Modeling Human Disease node of the IGTC are designed to trap all genes independent of expression (Stanford et al. 2006). This and the international functional genomic effort to generate targeted mutations in all genes (International Mouse Knockout Consortium 2007) are adding new X-linked mutations to the mouse mutant resource. In principle, using this screening method in combination with newer mutant mESC resources should make it possible to assess the embryonic phenotype of every gene on the mouse X chromosome. While this goal would require the coordinated efforts of several research centers, it would represent a major contribution to functional analysis of the X chromosome.

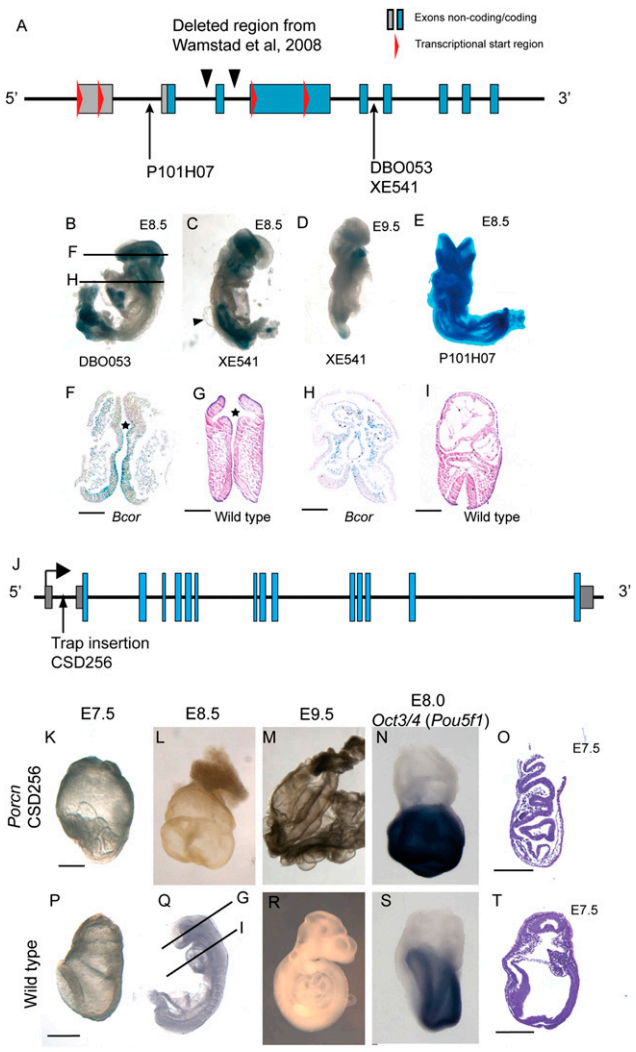

Figure 3. Analysis of Bcor and Porcn early embryo phenotypes. (*A*) Diagram of *Bcor* gene locus with locations of gene trap alleles, the conditional targeted allele as reported by Wamstad et al. (2008), and transcriptional start sites (red triangles). (*B–E*) mESC-derived embryos from three different *Bcor* GTs stained for *lacZ* expression. (*B*) Embryo from DB0053 cell line, used for histological analysis in *F* and *H*. Note the small head and heart, and truncated tail bud compared with controls (*Q*,*R*). (*C*) E8.5 mESC-derived embryo from XE541 cell line. Note the similar appearance and expression to DB0053 line. Also shown is a cyst (arrowhead) on the dorsal region of the embryo flanking the neural tube. (*D*) E9.5 *Bcor* mutant embryo stained for *lacZ* expression; of note is the severe posterior truncation, and small head and heart compared with wild-type controls (*Q*,*R*). (*E*) E8.5 embryo from P101H07 cell line exhibits exencephaly. (*F*) Transverse histological section of *Bcor* mutant embryo (*B*) head showing poor formation of optic pits (star), compared with an equivalent region from a wild-type stage-matched embryo (*G*). (*H*) Transverse histological section through heart field of *Bcor* mutant embryo (*C*) compared with equivalent region in stage-matched embryo (*I*). *Bcor* mutants (*H*) have a small symmetrical heart compared with the looped asymmetrical heart of controls (*I*). Also, *Bcor* mutants have an open neural tube compared with control embryos. (*F–I*) Scale bar, 100 μm. (*J*) Schematic of *Porcn* gene locus showing exons and GT insertion in first intron. (*K–N*) *Porcn* fully mESC-derived embryos. (*P–S*) Stage-matched wild-type embryos. (*K*) At E7.5, the *Porcn* null epiblast is highly folded and accumulates in the amniotic cavity compared to wild-type embryos (*P*). (*L*) At E8.5, *Porcn* mutants have no head, heart, allantois, or somite structures compared with stage-matched controls (*Q*). (*M*) At E9.5, *Porcn* mutant embryos consist of a yolk sac and small cyst-like structures, compared with wild-type controls that have a fully formed embryo body axis (*R*). (*N*) At E7.75 head-fold stage, *Porcn* mutant embryos fail to down-regulate *Pou5f1* compared with stage-matched controls (*S*). (*O*) Hematoxylin and eosin-stained sagittal section along the presumed anterior posterior axis of *Porcn* mutants reveals details of highly folded epiblast and epiblast vesicles compared with the smooth epiblast of controls at E7.75 (*T*). *Porcn* mutants had no morphological node apparent in any of the sections from two mutant E7.5 embryos examined; also, the visceral endoderm does not appear to be displaced from the embryonic region of *Porcn* mutants. (*K*,*P*,*O*,*T*) Scale bar, 200 μm.

Table 3. Known human and mouse phenotypes and associated mutations

Mouse gene symbol	Human disease (OMIM)	Human phenotype	Mouse phenotype	Mutation comments
Atrx	ATRX (301040) (1995)	Mental retardation, facial abnormalities	Normal embryos	No reported embryonic lethality in humans.
Bcor	OFCD (300166) (2004)	Male lethal; microphthalmia (small eyes), mental retardation, dental and pallet abnormalities, skeletal deformities, variable cardiac and laterality defects	Forebrain fusion, midline defects, cardiac defects, posterior truncation	Recapitulated male lethality in humans.
Brwd3	MRX 93 (30065) (2007)	Mental retardation, macrocephaly, muscular hypotonia	Normal embryos	Expression in heart and brain.
Cul4b	Cabazes syndrome (300354), MRX 15 (300639) (2007)	Mental retardation	Incomplete turning, defective neurulation, shorted posterior axis, swollen pericardium, and stalled cardiac development	No reported null in humans, only C terminal truncations. Gene trap is fully null.
Dlg3	MRX 90 (300189)(2004)	Mental retardation	Forebrain deletion, severe posterior truncation, and an absence of embryonic turning	Human mutation is splice donor. Mouse is null.
Flna	OPD1, OPD2, and frontometaphyseal dysplasia (300017) (1998-2001)	Male lethal; females malformations of the head and face, skeleton, brain, and urogenital tract	Normal embryos	More 3′ mutations associated with male survival and milder symptoms in females. Gene trap is very 3′ in gene.
Huwe1	MRX17 (300705); Tuner Type mental retardation (300706) (2008)	Mental retardation and macrocephaly	Posterior truncations, gastrulation defects	No null or truncation mutations observed in humans, only point mutations or gene duplications.
Kdm5c	MRSXJ (300534) (2005)	Mental retardation	Cardiac looping defect	May have alternate translational start, gene trap blocks majority of transcription.
Porcn	FDH (305600) (2007)	Male lethal; lateral skin lesion, hair loss, fused and extra digits, mental retardation, microphthalmia, dental and pallet disorders	Failed gastrulation, failed differentiation of the epiblast	Recapitulated male lethality in humans.

Overall, the integration of our data set with the OMIM data set will produce an important resource for both the biological and clinical communities to identify the molecular causes of human genetic disease. The data set will also expand our understanding of the role of the X chromosome during embryonic development.

Methods

Selection and verification of ES lines

A multistep approach was used to select all trapped genes on the X chromosome. First, sequence tags for all available GT lines were obtained from the IGTC database. These tags were then blasted against a library of mRNA sequences with chromosomal and genetic locations from the mouse. BLAST (Altschul et al. 1990) scores had to be below E^{-30} sequences and have >95% identity over the span of the tag to be considered a match to a gene. The next selection criterion was that the trap deleted >50% of the gene. From this list, mouse genes with synteny to the human X chromosome were selected. Finally, any gene that had been mutated in mice or was known to be associated with a human disease was removed to generate a final list of genes for screening. In some cases, multiple cell lines per gene were used to test the specificity of observed phenotypes as well as the differences in insertion position and phenotype.

Confirmation of the GT integration site, as mapped by the German Gene Trap Consortium (GGTC), BayGenomics via Mutant Mouse Regional Resource Center (MMRRC), or Center for Modeling Human Disease (CMHD) GT node, was done by RT-PCR. Primers were designed in an exon directly before the trap, or, if no appropriate primer was available, an exon further upstream was used. A primer was also placed in the GT as supplied by the GT resource group. Lastly, a primer was placed in an exon 3′ of the trap to test for the presence of normal transcripts. In cases where the PCR fragment size was not close to the expected size, the PCR product was sequenced to confirm the PCR product. mRNA from wild-type cells was used as a negative control for the trapped transcript and as a positive control for the wild-type transcript. All primers are listed in Supplemental Table 3. RNA was isolated from a 6-cm dish of mESCs using TRIzol (Invitrogen) and dissolved in 30 μL of DEPC water. Two micrograms of total RNA was used for reverse transcription, which was performed with the SuperScript II Reverse Transcriptase kit (Invitrogen) and primed with random octamers. From a final reverse transcription reaction volume of 20 μL, 1 μL was used for subsequent PCR analysis. PCR extension times and annealing temperatures were optimized for each transcript. Each line was tested for mycoplasm infection and confirmed negative prior to aggregation.

Culture of ES lines

Cell lines were thawed and expanded on a feeder layer of Mitomycin C-inactivated mouse embryonic fibroblasts (MEFs) using standard protocols (Joyner 2000). mESC media contained high glucose DMEM supplemented with 15% FBS (tested to support generation of chimeras; Hyclone), 1000 U/mL LIF, 2 mM GlutaMAX (Invitrogen), 1 mM Na pyruvate (Invitrogen), 0.1 mM nonessential amino acids (Invitrogen), 50 U/mL penicillin and streptomycin

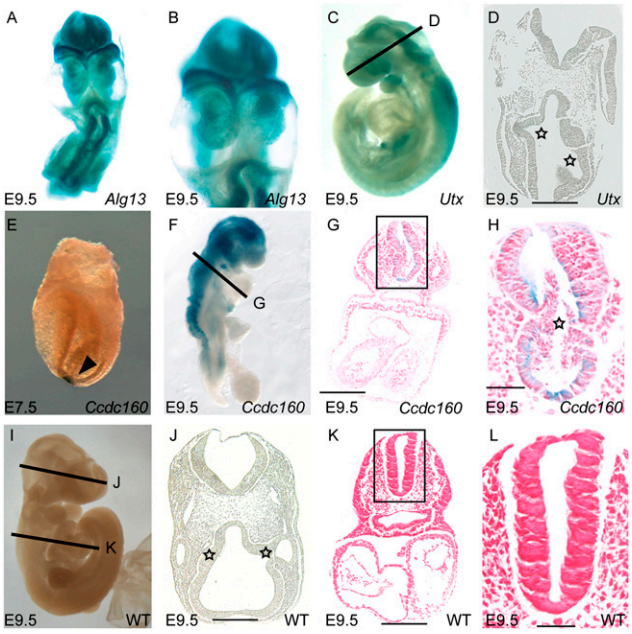

Figure 4. Novel embryonic phenotypes. (*A,B*) *Alg13* mutants have widespread expression of the *lacZ* reporter, are severely developmentally delayed, and have cardia bifida. (*C*) *Kdm6a* mutant embryos have an open head and *lacZ* reporter expression in the head and neural tube. (*D*) Histological analysis of heads of *Kdm6a* mutants shows a fused forebrain and uneven, delayed optic pits (stars), compared with a similar region in a stage-matched control embryo (*J*). (*E*) *Ccdc160* mutant embryos have expression in the node at E7.5. (*F*) At E9.5, expression of *Ccdc160* has become highly restricted to the developing brain and neural tube. (*G*) Histological analysis of an E9.5 *Ccdc160* mutant embryo revealed the presence of cells in the lumen of the neural tube; this was observed in three out of three embryos examined (data not shown). (*H*) Closer view of the neural tube in *G* highlighting the trapped cells (star). (*I*) A wild-type E9.5 embryo has a single folded heart and closed head. (*J*) Histological section of the head of an E9.5 wild-type embryo showing segmented developing brain and symmetrical optic pits (stars). (*K*) Histological section though a wild-type E9.5 embryo showing normal number of developing chambers and a closed neural tube with an empty lumen (star). (*L*) Higher magnification view of neural tube in *K*.

(Invitrogen), and 0.1 mM 2-mercaptoethanol (Invitrogen). Cells were fed daily and passaged every 2 d. Each cell line was tested for mouse pathogens (Research Animal Diagnostics Laboratory [RADIL]) prior to use for aggregation.

Aggregation assays

Tetraploid embryos

Embryos at the two-cell stage were collected at E1.5 from superovulated ICR (Harlan) or BDF1 (Charles River) mice mated with ICR, BDF1, or B5/EGFP [Tg(CAG-EGFP)B5Nagy] (Hadjantonakis et al. 1998), eYFP (7AC5/EYFP) [Tg(CAG-EYFP)7AC5Nagy] (Hadjantonakis et al. 2002), or DsRed*MST [Tg(CAG-DsRed*MST)1Nagy] (Vintersten et al. 2004) males and electrofused to generate tetraploid embryos (Nagy 2003). The fused, tetraploid embryos were cultured in microdrops of KSOM with amino acids (Millipore) under mineral oil at 37°C in 94% air/6% CO_2. Twenty-four hours after fusion the tetraploid embryos that developed to four-cell stage embryos were used for aggregation. Zonae pellucidae of the embryos were removed by treatment with acid Tyrode's solution (Sigma). mESCs were briefly trypsinized to form clumps of loosely connected cells, and clumps of eight to 15 mESCs were placed between two zona-free tetraploid embryos in depression wells made in the plastic dish. These aggregates were cultured overnight in KSOM microdrops before morulae and blastocysts were transferred into the uteri of 2.5-d pseudopregnant recipients.

Diploid embryos

Superovulated ICR (Harlan) female mice were mated with male mice homozygous for a ubiquitously expressed transgene coding for eGFP (B5/EGFP) [Tg(CAG-EGFP)B5Nagy] (Hadjantonakis et al. 1998), eYFP (7AC5/EYFP) [Tg(CAG-EYFP)7AC5Nagy] (Hadjantonakis et al. 2002), or DsRed*MST [Tg(CAG-DsRed*MST)1Nagy] (Vintersten et al. 2004). Embryos were collected at day E1.5 and cultured overnight in microdrops of KSOM with aminoacids (Millipore) under mineral oil at 37°C in 94% air/6% CO_2 until the uncompacted eight-cell stage. The next morning each embryo was aggregated with a clump of eight to 15 mES cells in depression wells and cultured one more night in KSOM microdrops, then morulae and blastocysts were transferred into the uteri of pseudopregnant females at E2.5 as described (Nagy 2003).

Phenotypic analysis

Embryos from diploid aggregations were dissected at day E9.5 and screened for host embryo contribution. Only embryos with no host contribution, aside from the typical hindgut contribution, were used (Kwon et al. 2008; Burtscher and Lickert 2009). An initial morphological assessment determined if there was any obvious phenotypic difference between the mESC-derived embryos, chimeric, and fully host-derived embryos. Embryos were fixed and processed for *lacZ* staining. After *lacZ* staining the embryos were again assessed for staining patterns and morphology.

Embryos from tetraploid aggregations were screened in two stages. In the first stage mESC were aggregated with ICR or BDF1 tetraploid embryos, dissected at E7.5, E8.5, and E9.5, and compared with controls to assess any morphological defect. ES cell clones that gave either patchy *lacZ* staining (an indication of chimerism with host cells) or constant phenotypes were validated in a second screen. In the second screen the ES cells were again aggregated with tetraploid embryos, but using CD-1 females that ubiquitously expressed a fluorescent marker (dsRed*MST, eGFP, or eYFP) to exclude tetraploid cell contribution to the embryo.

For *lacZ*, embryos to be stained (E6.5–E11.5) were fixed in PBS (pH 7.3) containing 0.02% NP-40, 5 mM EGTA (pH 8.0), 2 mM $MgCl_2$, 1% formaldehyde, and 0.2% glutaraldehyde for 30 min at room temperature, washed three times with 0.02% NP-40 in PBS, and then placed in X-gal staining solution (PBS at pH 7.3 containing 0.02% NP-40, 2 mM $MgCl_2$, 5 mM $K_3[Fe(CN)_6]$, 5 mM $K_4[Fe(CN)_6] \times 6H_2O$, 0.01% sodium deoxycholate, 1 mg/mL X-gal). Staining was carried out in the dark, overnight at room temperature. After staining, samples were washed in PBS and stored in 4% paraformaldehyde at 4°C. Whole-0mount in situ hybridization was performed as described previously (Tamplin et al. 2008).

All mouse mutant embryos were digitally imaged regardless of *lacZ* staining pattern or body morphology. Image data were stored in a relational database. Embryos were imaged in PBS on a stereo fluorescence microscope (Leica MZ16F) and attached digital camera (QIMAGING MicroPublisher 5.0RTV); raw images were processed with Volocity5 software or a Zeiss SteREO Lumar.V12 microscope using an AxioCam MRc5 camera.

Embryos were sectioned by the Center for Modeling Human Disease core histology facility at the Toronto Center for Phenogenomics. Slides of embryo sections were imaged on a ZEISS scanner (MIRAX SCAN), and single images were captured in MIRAX VIEWER 1.11 software and processed in Adobe Photoshop CS2.

Database construction

An internal database was constructed with File Maker Pro 8.5. All data were manually entered and curated in the database. Tables were then exported from the internal database to construct the online version using MySQL, Java, Php, and HTML.

Acknowledgments

We thank Jorge Cabezas, Suzanne MacMaster, and Sandra Tondat from the Toronto Center for Phenogenomics; and Patrizia Giallonardo, Adrianne Tasdemir, and Susanne Weidemann for technical support in generating aggregation embryos. We also thank Valerie Prideaux for assistance with FileMakerPro and Christine To for programming assistance in the generation of the online version of the phenotype database. We thank Les Biesecker for sequencing of *KLF8* in carriers of TARPS at our request. We thank Thomas Kislinger and Chi-Chung Hui for critical reading of the manuscript and Jean Cox for editorial assistance. This work was supported in part by the March of Dimes (grant no. 6-FY06-364 and 6-FY08-315) to J.R. H.L. is supported by the German research foundation and the Helmholtz society. W.W. and R.K. are funded by the NGFN-Plus (FKZ: 01GS0858/01GS0823) and by the EU, FP6 (EUCOMMEU-COMM: LSHM-CT-2005-018931).

References

Altschul SF, Gish W, Miller W, Myers EW, Lipman DJ. 1990. Basic local alignment search tool. *J Mol Biol* **215:** 403–410.

Andersen JS, Wilkinson CJ, Mayor T, Mortensen P, Nigg EA, Mann M. 2003. Proteomic characterization of the human centrosome by protein correlation profiling. *Nature* **426:** 570–574.

Burtscher I, Lickert H. 2009. Foxa2 regulates polarity and epithelialization in the endoderm germ layer of the mouse embryo. *Development* **136:** 1029–1038.

Cuthbert PC, Stanford LE, Coba MP, Ainge JA, Fink AE, Opazo P, Delgado JY, Komiyama NH, O'Dell TJ, Grant SG. 2007. Synapse-associated protein 102/dlgh3 couples the NMDA receptor to specific plasticity pathways and learning strategies. *J Neurosci* **27:** 2673–2682.

Fan Z, Yamaza T, Lee JS, Yu J, Wang S, Fan G, Shi S, Wang CY. 2009. BCOR regulates mesenchymal stem cell function by epigenetic mechanisms. *Nat Cell Biol* **11:** 1002–1009.

Field M, Tarpey PS, Smith R, Edkins S, O'Meara S, Stevens C, Tofts C, Teague J, Butler A, Dicks E, et al. 2007. Mutations in the BRWD3 gene cause X-linked mental retardation associated with macrocephaly. *Am J Hum Genet* **81:** 367–374.

Friedrich G, Soriano P. 1991. Promoter traps in embryonic stem cells: A genetic screen to identify and mutate developmental genes in mice. *Genes Dev* **5:** 1513–1523.

Gao XD, Tachikawa H, Sato T, Jigami Y, Dean N. 2005. Alg14 recruits Alg13 to the cytoplasmic face of the endoplasmic reticulum to form a novel bipartite UDP-N-acetylglucosamine transferase required for the second step of N-linked glycosylation. *J Biol Chem* **280:** 36254–36262.

Garrick D, Sharpe JA, Arkell R, Dobbie L, Smith AJ, Wood WG, Higgs DR, Gibbons RJ. 2006. Loss of Atrx affects trophoblast development and the pattern of X-inactivation in extraembryonic tissues. *PLoS Genet* **2:** e58. doi: 10/1371/journal.pgen.0020058.

Greenfield A, Carrel L, Pennisi D, Philippe C, Quaderi N, Siggers P, Steiner K, Tam PP, Monaco AP, Willard HF, et al. 1998. The UTX gene escapes X inactivation in mice and humans. *Hum Mol Genet* **7:** 737–742.

Grzeschik KH, Bornholdt D, Oeffner F, Konig A, del Carmen Boente M, Enders H, Fritz B, Hertl M, Grasshoff U, Hofling K, et al. 2007. Deficiency of PORCN, a regulator of Wnt signaling, is associated with focal dermal hypoplasia. *Nat Genet* **39:** 833–835.

Hadjantonakis AK, Gertsenstein M, Ikawa M, Okabe M, Nagy A. 1998. Generating green fluorescent mice by germline transmission of green fluorescent ES cells. *Mech Dev* **76:** 79–90.

Hadjantonakis AK, Macmaster S, Nagy A. 2002. Embryonic stem cells and mice expressing different GFP variants for multiple non-invasive reporter usage within a single animal. *BMC Biotechnol* **2:** 11. doi: 10.1186/1472-6750-2-11.

Hilton E, Johnston J, Whalen S, Okamoto N, Hatsukawa Y, Nishio J, Kohara H, Hirano Y, Mizuno S, Torii C, et al. 2009. BCOR analysis in patients with OFCD and Lenz microphthalmia syndromes, mental retardation with ocular anomalies, and cardiac laterality defects. *Eur J Hum Genet* **17:** 1325–1335.

International Knockout Mouse Consortium. 2007. A mouse for all reasons. *Cell* **128:** 9–13.

Joyner AL. 2000. *Gene targeting: A practical approach*. Oxford University Press, Oxford.

Kawaji H, Kasukawa T, Fukuda S, Katayama S, Kai C, Kawai J, Carninci P, Hayashizaki Y. 2006. CAGE Basic/Analysis Databases: The CAGE resource for comprehensive promoter analysis. *Nucleic Acids Res* **34:** D632–D636.

Kurpinski KT, Magyari PA, Gorlin RJ, Ng D, Biesecker LG. 2003. Designation of the TARP syndrome and linkage to Xp11.23-q13.3 without samples from affected patients. *Am J Med Genet A* **120A:** 1–4.

Kwon GS, Viotti M, Hadjantonakis AK. 2008. The endoderm of the mouse embryo arises by dynamic widespread intercalation of embryonic and extraembryonic lineages. *Dev Cell* **15:** 509–520.

Lanasa MC, Hogge WA, Kubik CJ, Ness RB, Harger J, Nagel T, Prosen T, Markovic N, Hoffman EP. 2001. A novel X chromosome-linked genetic cause of recurrent spontaneous abortion. *Am J Obstet Gynecol* **185:** 563–568.

Lee MG, Villa R, Trojer P, Norman J, Yan KP, Reinberg D, Di Croce L, Shiekhattar R. 2007. Demethylation of H3K27 regulates polycomb recruitment and H2A ubiquitination. *Science* **318:** 447–450.

Liu P, Wakamiya M, Shea MJ, Albrecht U, Behringer RR, Bradley A. 1999. Requirement for Wnt3 in vertebrate axis formation. *Nat Genet* **22:** 361–365.

Mitchell KJ, Pinson KI, Kelly OG, Brennan J, Zupicich J, Scherz P, Leighton PA, Goodrich LV, Lu X, Avery BJ, et al. 2001. Functional analysis of secreted and transmembrane proteins critical to mouse development. *Nat Genet* **28:** 241–249.

Morkel M, Huelsken J, Wakamiya M, Ding J, van de Wetering M, Clevers H, Taketo MM, Behringer RR, Shen MM, Birchmeier W. 2003. Beta-catenin regulates Cripto- and Wnt3-dependent gene expression programs in mouse axis and mesoderm formation. *Development* **130:** 6283–6294.

Nagy A. 2003. *Manipulating the mouse embryo. A laboratory manual*. Cold Spring Harbor Laboratory Press, Cold Spring Harbor, NY.

Nagy A, Gocza E, Diaz EM, Prideaux VR, Ivanyi E, Markkula M, Rossant J. 1990. Embryonic stem cells alone are able to support fetal development in the mouse. *Development* **110:** 815–821.

Ng D, Thakker N, Corcoran CM, Donnai D, Perveen R, Schneider A, Hadley DW, Tifft C, Zhang L, Wilkie AO, et al. 2004. Oculofaciocardiodental and Lenz microphthalmia syndromes result from distinct classes of mutations in BCOR. *Nat Genet* **36:** 411–416.

Nord AS, Chang PJ, Conklin BR, Cox AV, Harper CA, Hicks GG, Huang CC, Johns SJ, Kawamoto M, Liu S, et al. 2006. The International Gene Trap Consortium Website: A portal to all publicly available gene trap cell lines in mouse. *Nucleic Acids Res* **34:** D642–D648.

Pegoraro E, Whitaker J, Mowery-Rushton P, Surti U, Lanasa M, Hoffman EP. 1997. Familial skewed X inactivation: A molecular trait associated with high spontaneous-abortion rate maps to Xq28. *Am J Hum Genet* **61:** 160–170.

Poueymirou WT, Auerbach W, Frendewey D, Hickey JF, Escaravage JM, Esau L, Dore AT, Stevens S, Adams NC, Dominguez MG, et al. 2007. F0 generation mice fully derived from gene-targeted embryonic stem cells allowing immediate phenotypic analyses. *Nat Biotechnol* **25:** 91–99.

Ross MT, Grafham DV, Coffey AJ, Scherer S, McLay K, Muzny D, Platzer M, Howell GR, Burrows C, Bird CP, et al. 2005. The DNA sequence of the human X chromosome. *Nature* **434:** 325–337.

Sanchez C, Sanchez I, Demmers JA, Rodriguez P, Strouboulis J, Vidal M. 2007. Proteomics analysis of Ring1B/Rnf2 interactors identifies a novel complex with the Fbxl10/Jhdm1B histone demethylase and the Bcl6 interacting corepressor. *Mol Cell Proteomics* **6:** 820–834.

Schnutgen F, De-Zolt S, Van Sloun P, Hollatz M, Floss T, Hansen J, Altschmied J, Seisenberger C, Ghyselinck NB, Ruiz P, et al. 2005. Genomewide production of multipurpose alleles for the functional analysis of the mouse genome. *Proc Natl Acad Sci* **102:** 7221–7226.

Stanford WL, Epp T, Reid T, Rossant J. 2006. Gene trapping in embryonic stem cells. *Methods Enzymol* **420:** 136–162.

Tamplin OJ, Kinzel D, Cox BJ, Bell CE, Rossant J, Lickert H. 2008. Microarray analysis of Foxa2 mutant mouse embryos reveals novel gene expression and inductive roles for the gastrula organizer and its derivatives. *BMC Genomics* **9:** 511. doi: 10.1186/1471-2164-9-511.

Tanaka K, Okabayashi K, Asashima M, Perrimon N, Kadowaki T. 2000. The evolutionarily conserved porcupine gene family is involved in the processing of the Wnt family. *Eur J Biochem* **267:** 4300–4311.

Tarpey P, Parnau J, Blow M, Woffendin H, Bignell G, Cox C, Cox J, Davies H, Edkins S, Holden S, et al. 2004. Mutations in the DLG3 gene cause nonsyndromic X-linked mental retardation. *Am J Hum Genet* **75:** 318–324.

Tarpey PS, Smith R, Pleasance E, Whibley A, Edkins S, Hardy C, O'Meara S, Latimer C, Dicks E, Menzies A, et al. 2009. A systematic, large-scale resequencing screen of X-chromosome coding exons in mental retardation. *Nat Genet* **41:** 535–543.

Vintersten K, Monetti C, Gertsenstein M, Zhang P, Laszlo L, Biechele S, Nagy A. 2004. Mouse in red: Red fluorescent protein expression in mouse ES cells, embryos, and adult animals. *Genesis* **40:** 241–246.

Wamstad JA, Corcoran CM, Keating AM, Bardwell VJ. 2008. Role of the transcriptional corepressor Bcor in embryonic stem cell differentiation and early embryonic development. *PLoS ONE* **3:** e2814. doi: 10.1371/journal.pone.002814.

Wang X, Reid Sutton V, Omar Peraza-Llanes J, Yu Z, Rosetta R, Kou YC, Eble TN, Patel A, Thaller C, Fang P, et al. 2007. Mutations in X-linked PORCN, a putative regulator of Wnt signaling, cause focal dermal hypoplasia. *Nat Genet* **39:** 836–838.

Yamanaka Y, Tamplin OJ, Beckers A, Gossler A, Rossant J. 2007. Live imaging and genetic analysis of mouse notochord formation reveals regional morphogenetic mechanisms. *Dev Cell* **13:** 884–896.

Received January 11, 2010; accepted in revised form May 11, 2010.